RSC Advances

RSC Publishing

PAPER

View Article Online
View Journal | View Issue

Controlled biosilification using self-assembled short peptides A_6K and V_6K†

Cite this: *RSC Advances*, 2013, **3**, 2784

Qinrong Wang,[a] Jun Yu,[a] Xin Zhang,*[a] Daojun Liu,[b] Jinhong Zheng,[b] Ying Pan[b] and Yuejuan Lin[c]

Received 10th September 2012,
Accepted 18th December 2012

DOI: 10.1039/c2ra22099g

www.rsc.org/advances

We report the molecular self-assembly of two amphiphilic peptides (A_6K and V_6K) and the application of their self-assemblies as organic templates to direct biosilica formation. Under ambient conditions, A_6K self-assembled into nanotubes 2.7 nm tall and approximately 1 μm to 2 μm long. In contrast, V_6K self-assembled into lamellar-stack nanostructures approximately 4 nm tall and under 100 nm long. The self-assembled peptide nanostructures were used as organic templates to direct biosilica formation. Comparing with the self-assembled structures formed by the peptide/anions system, novel silica morphologies can be obtained by changing the peptide composition, using different anions, and applying electrostatic/flow fields. We observed that the presence of anions is important but not enough to produce ordered silica structures with novel morphologies. This study provides further understanding of silica biomineralization tailored by assembled peptides, which offers a simple but efficient method to control the formation of inorganic material.

1 Introduction

In past decades, the molecular self-assembly approach has been applied to fabricate novel functional materials and biomimetic nanostructures because of their biocompatibility, chemical modifiability, and high efficiency.[1–7] Among the emerging self-assembling molecules, amphiphilic peptides, with their simple design and multiple driving forces, have drawn research interest for their wide range of biomedical and technological applications in controlled release medicine, as structural templates for inorganic materials, and as tissue scaffolds.[6,8–18] Compared with conventional surfactants, hydrogen bonding and hydrophobic and electrostatic interactions are the typical major driving forces that regulate the self-assembly process of amphiphilic peptides.[17,18] Amphiphilic peptides are ideal templates to tailor the synthesis of ordered inorganic materials under ambient conditions because of their biocompatibility and well-defined self-assembled morphologies.[19,20]

Biotemplated fabrication offers unique directions for the controlled growth and assembly of inorganic materials.[21–23] Considerable progress has been achieved in the biomimetic synthesis of biosilica using the self-assemblies of amphiphilic peptides. For example, Hartgerink *et al.*[24] synthesized silica nanotubes with tunable dimensions through the condensation of tetraethoxysilane (TEOS) on peptide-amphiphile nanofiber templates and demonstrated that only peptide amphiphiles that contain lysine, histidine or glutamic acid are positive catalytic templates. Xu *et al.*[25–27] designed and controlled the self-assembly of an ultrashort peptide (I_3K) into stable nanotubes, which were used as templates for the precise formation of silica nanotubes. The morphology and nanostructures of the silica nanomaterials were easily regulated by changing the ratio of peptide to silica precursor, pH, and the aging periods. These investigations inspired us to design advanced materials *via* molecular self-assemblies as organic templates. However, compared with the extensive investigations on short peptide self-assembly, the selection of self-assembled short peptides as organic templates to tailor biosilica fabrication is not well developed. A detailed understanding of the mechanisms behind the controlled formation of silica is also not clearly understood.[28,29] Thus, determining the structural details of the biomimetic process is extremely important to address a series of issues, such as the relationships between the molecular structures of the peptides and the novel biosilica structures with controlled morphologies and the prediction of the resulting biosilica structures based on molecular architecture.

In this study, the peptide-based self-assemblies formed from A_6K and V_6K were used as organic templates to direct biosilica deposition and thus gain better insight into the mediation of peptide self-assembly on biosilica formation. Several chemical/physical factors such as the type of hydrophobic amino acid, the nature of the peptide/anion complex, pH, and external electrostatic/flow fields that affect biosilica

[a]*Department of Chemistry, Science Faculty, Shantou University, Shantou, 515063, China. E-mail: xzhang@stu.edu.cn; Fax: 86 754 82903639*
[b]*Medical College, Shantou University, Shantou, 515041, China*
[c]*Analysis & Testing Center, Shantou University, Shantou, 515063, China*
† Electronic supplementary information (ESI) available. See DOI: 10.1039/c2ra22099g

morphologies were systematically investigated. Despite the short structures of these two amphiphilic peptides, their properties are similar to those of conventional long aliphatic chain surfactants. The biosilica morphologies were controlled by different methods using the A_6K and V_6K self-assemblies. These methods are useful to further explore the biological application of short peptides.

2. Experimental section

2.1 Materials

Protected amino acids (Fmoc-L-Ala-OH, Fmoc-L-Val-OH, and Fmoc-L-Lys(Boc)-OH) for peptide synthesis were purchased from GL Biochem Ltd. (Shanghai, China) and use as received, unless specified. All other reagents were obtained from Sigma-Aldrich Chemical Company (USA). Dichloromethane and dimethylformamide were redistilled and subsequently dried with molecular sieves prior to peptide synthesis. Water was processed by a Millipore purification system with a minimum resistivity of 18.0 MΩ cm.

2.2 Peptide synthesis

The short amphiphilic peptides A_6K and V_6K (A, alanine; V, valine; K, lysine) were synthesized on a CEM liberty microwave synthesizer using the general procedure for Fmoc chemistry of solid-phase peptide synthesis.[10,18] Rink amide resin was used to allow C-terminal amidation. The N-terminus was capped with acetic anhydride before cleavage from the resin, resulting in the molecule having only one positive charge from the side chain of the lysine residue at neutral pH. After rotary evaporation, the cleaved peptides were purified by deposition with copious cold ether at least six times and centrifuged to keep the pH constant at 5–6. Then, the final peptide products were lyophilized for 2 days to reach a high purity of over 95% based on reversed-phase HPLC and ESI-MS (Fig. S1, ESI†). The measurements were performed using Waters 2695 Alliance HPLC system and Finnigan Mat TSQ 7000 instruments, respectively.

2.3 Preparation of peptide solutions

The peptide stock and salt solutions were prepared by directly dissolving the dry samples in pure water until no visible precipitates were observed. The peptide solution (A_6K, 3 mM; V_6K, 0.6 mM) and appropriate salt solution (5.0×10^{-2} M) were mixed to reach the required concentrations. All peptide stock solutions were aged for at least a week at room temperature, and then used for characterization and biosilica synthesis.

2.4 Biosilification under different conditions

Biosilica synthesis was performed as previously described.[30–34] The stock solution of silicic acid was prepared *via* ultrasonication of TEOS in HCl (1 mM) for 10 min. 100 μL of peptide solution was premixed with 300 μL sodium phosphate for 5 min before a certain volume of freshly prepared silicic acid was added. High silica acid concentrations were found to increase the level of nontemplated deposition, whereas low silica acid concentrations favored the formation of regular morphologies of biosilica. However, the template was coated with a thin silica layer if the silica acid concentrations were below a certain value. Thus, the TEOS concentration was kept constant at 20 mM to obtained biosilica structures with controlled morphologies (Fig. S2, ESI†). After the desired reaction time elapsed, the samples were centrifuged at 14 000 rpm for 10 min. The supernatant was then removed, and the white precipitate was rinsed with distilled water and ethanol three times to remove unreacted TEOS as well as the residual peptide. To investigate the effect of counterions, the aforementioned procedures were repeated, and sodium phosphate was replaced with aqueous sodium sulfate or sodium carbonate solution. This dispersion was further diluted, and a few drops of the solution formed were placed on scanning electron microscope (SEM) sample holders, and then left to dry under ambient conditions.

For the electric field peptide deposition tests, a 4 V electric potential was applied. Once the externally applied electrostatic field was deactivated, the cathode electrode surface was washed with sodium phosphate solution to remove any free polypeptides unattached to the cathode electrode surface. Silicic acid was then placed onto the flat cathode electrode surface and allowed to react with the polypeptide-patterned surface for 1 to 2 min. The cathode electrode surface was washed with double-distilled deionized water prior to imaging. For the flow field deposition tests, a hydrodynamic flow field, which directs the formation of a biosilica-like morphology at a rate of 10 mL min^{-1}, was generated in a lab-built flow reactor 1.5 cm wide and 5 cm long. The peptide solution was injected into the reaction vessel, and then the freshly prepared silicic acid was added after N_2 had flowed into the reactor for 5 min. During the reaction periods, we controlled the flow rate by adjusting the flow control valve to keep the designed flow condition in the reactor. After the required reaction time elapsed, the samples were centrifuged at 14 000 r min^{-1} for 10 min. The supernatant was subsequently removed, and the precipitate was washed with distilled water and ethanol three times to remove unreacted TEOS and the residual peptide.

2.5 Sample characterization

Atomic force microscope (AFM). AFM measurements were performed under mild conditions using a Nanoscope IIIa Multimode atomic force microscope (America Digital Instrument Co.) in tapping mode. For sample preparation, 5 μL to 10 μL of peptide solutions were deposited onto a freshly cleaved mica surface. After 10 to 30 s, excess liquid was removed from the mica surface, followed by drying with a gentle N_2 stream. After sample preparation, the mica surface was immediately subjected to AFM imaging. Topographic data were regularly recorded as 512 × 512 pixel images in trace and retrace directions simultaneously to check for scan artifacts. Image analysis was conducted using Digital Instruments Nanoscope software (version V530r3sr3). All images were flattened using a first-order line fit to remove any tilt in the surface.

Scanning electron microscopy (SEM). Sample imaging was performed using a JEOS JSM-6306 LA SEM operating at 10 kV. The samples were prepared by placing a small drop of the diluted dispersion on a mica substrate, which was then

allowed to dry under ambient conditions. The dried samples were subsequently sputtered with a thin gold layer under vacuum to a depth of 1 to 2 nm.

Circular dichroism (CD). CD spectra were recorded on an MOS 450 spectrophotometer (Biologic, France) in a 1 mm path length quartz cuvette in a single-cell mount setup. Background scans of the counterions (carbonate/sulfate/phosphate anions) and hydrolyzed TEOS solution were recorded and manually subtracted from the sample scans. A peptide solution in sodium carbonate, sodium sulfate, or sodium phosphate was mixed with the freshly hydrolyzed TEOS solution. The samples were then loaded into a 1 mm path length quartz cuvette to obtain the CD data. The data points for the wavelength-dependent CD spectra were recorded from 250 nm to 180 nm (at a rate of 50 nm min^{-1}) at every nanometer with a 1 nm bandwidth. Three scans for each of the duplicate samples were measured and averaged.

Fourier transformed infrared spectroscopy (FT-IR). All IR spectroscopy measurements were performed on a Nicolet iS5 IR spectrometer (Thermo Nicolet corporation, USA) using a thin potassium bromide (KBr) pellet as the sample holder. The spectroscopy instrument was continually purged with dry air for a minimum of 12 h prior to sample analysis. The resolution of the spectrum collection was set at 4 cm^{-1} and the scanning range was from 4000 cm^{-1} to 400 cm^{-1}.

Thermogravimetric analysis (TGA). TGA was conducted on a TGA 2050 analyzer (TA instruments). The dried samples were heated from 25 °C to 800 °C at a heating rate of 10 °C min^{-1} under a N_2 atmosphere. The observed mass loss was attributed to the quantitative pyrolysis of the peptide, with the remaining incombustible residues which are assumed to be pure silica.

3. Results and discussion

3.1 Self-assembly of A_6K and V_6K

As shown in Fig. 1a and 1b, the molecular structures of A_6K and V_6K comprise the hydrophobic moiety that consists of six

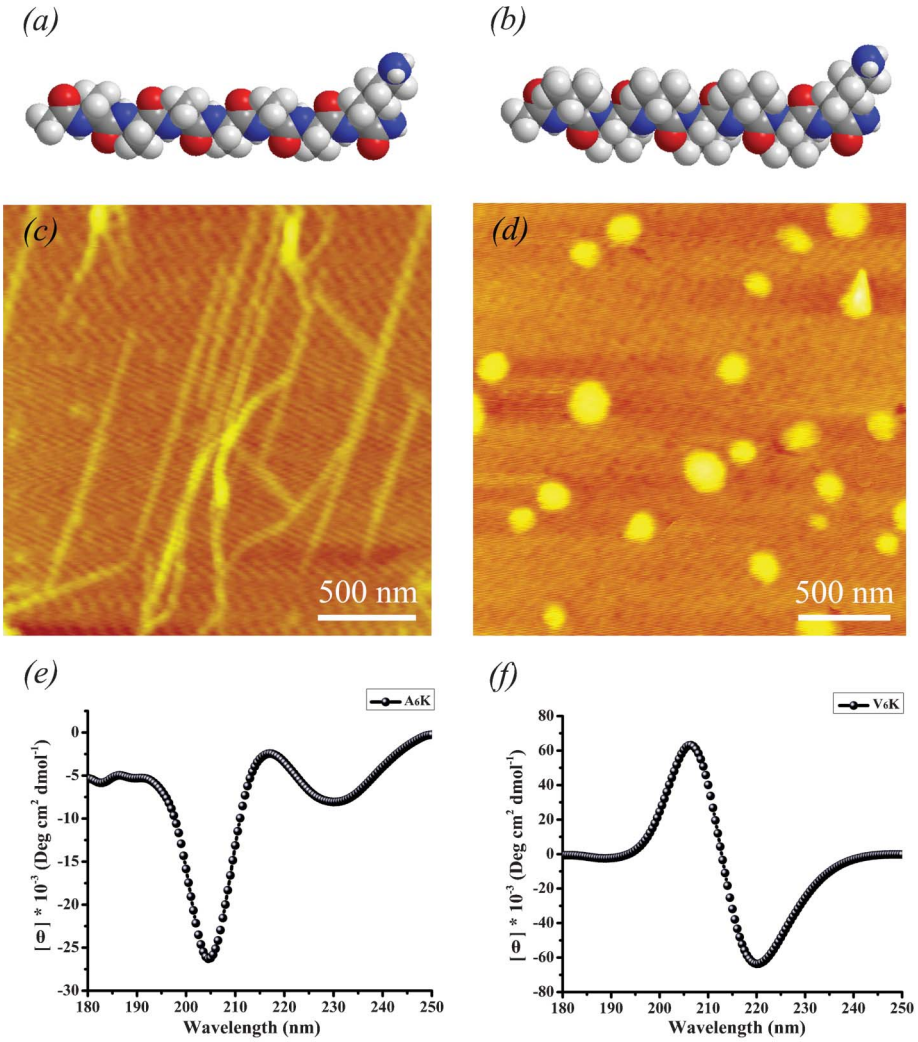

Fig. 1 Molecular structure of (a) A_6K and (b) V_6K. Color code: carbon, gray; hydrogen, white; oxygen, red; nitrogen, blue. The atomic force microscope (AFM) height images of the self-assembled structures formed by (c) A_6K at 3 mM in aqueous solution with a scan size of 2 × 2 μm^2 and a *Z* scale of 30 nm, and (d) V_6K at 0.6 mM in aqueous solution with a scan size of 2 × 2 μm^2 and a *Z* scale of 15 nm. Circular dichroism (CD) spectrum of (e) A_6K and (f) V_6K.

consecutive alanine/valine residues and the hydrophilic segment that contains a lysine residue. Such changes in molecular hydrophobicity enabled us to investigate the linkage between their molecular characteristics and nanostructures. Minor differences in the molecular structures of A and V have different influences on their morphologies. In pure water, A_6K and V_6K could readily self-assemble into stable nanofibers and lamellar stacks, respectively (Fig. 1c and 1d). Based on the corresponding AFM sectional profiles, A_6K formed long and uniform nanotubes that were 2.7 nm tall and approximately 1 to 2 μm long. However, V_6K molecules self-assembled into lamellar stacks approximately 4 nm tall and under 100 nm long (Fig. S3, ESI†). Molecular self-assembly is the spontaneous organization of molecules into well-defined morphologies. Generally, hydrophobic, electrostatic, and inter/intramolecular hydrogen-bonding interactions are considered as the dominant driving forces for the self-assembly process of surfactant-like peptides.[4,35–37] The positively charged hydrophilic regions of A_6K and V_6K were exposed to the surrounding water and experienced repulsion due to electrostatic forces. The synergistic effect of hydrophobic and electrostatic interactions controlled the self-assembly behavior. As the molecular hydrophobicity increased from A_6K to V_6K, these two peptides showed different aggregation abilities in aqueous solution. A_6K has a weaker aggregation ability and assembles into nanotubes. However, under similar conditions, V_6K forms stacks, which correspond to a lamellar bilayer with great interdigitation of its hydrophobic valine tails. Thus, these structural transitions from nanotubes to lamellar stacks caused by the combination of the electrostatic and hydrophobic interactions and by the tuning of the molecular structures of peptide amphiphiles affect the morphology of peptide self-assembly, which is consistent with previous reports on the self-assembly behavior of peptides by modifying peptide composition.[18,38,39]

The secondary structures of the peptides were characterized using the CD spectrum. As shown in Fig. 1e, the CD spectrum measured from the A_6K solution exhibits a negative peak near 205 nm and a negative absorption at around 228 nm, suggesting that the A_6K peptide mainly adopts a random coil conformation. However, substituting alanine with valine led to a progressive conformational change. In the case of V_6K, the CD spectrum reveals a typical β-sheet structure from the self-assembly system, characterized by a positive maximum at around 198 nm and a negative minimum at about 220 nm (Fig. 1f). Alanine and valine have different propensities in promoting secondary structures because of their electrostatic and hydrophobic interactions. Thus, changes in the peptide composition of A_6K and V_6K enabled us to investigate the linkage between their molecular characteristics and nanostructure. The self-assembly behavior of these two short peptides make them ideal for investigating possible factors that affect the dynamic self-assembly process and the potential to fabricate peptide-based inorganic morphologies with distinct structures.

3.2 Effect of different anionic counterions on the self-assembly of A_6K and V_6K

As shown in Fig. 2, different anions such as carbonates, sulfates, and phosphates are used to investigate their effects

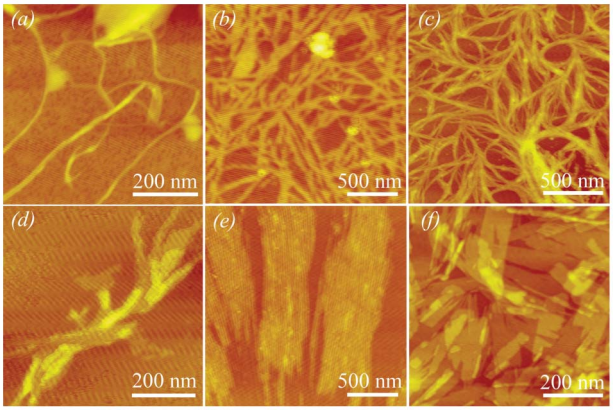

Fig. 2 AFM height images of the self-assembled nanostructures of A_6K in the presence of (a) sodium carbonate with a scanning size of 1.25 × 1.25 μm^2 and a *Z* scale of 30 nm; (b) sodium sulfate with a scan size of 1.65 × 1.65 μm^2 and a *Z* scale of 15 nm; (c) sodium phosphate with a scan size of 1.1 × 1.1 μm^2 and a *Z* scale of 15 nm. AFM height images of the self-assembled nanostructures of V_6K in the presence of (d) sodium carbonate with a scan size of 4 × 4 μm^2 and a *Z* scale of 20 nm; (e) sodium sulfate with a scan size of 1.5 × 1.5 μm^2 and a *Z* scale of 25 nm; (f) sodium phosphate with a scan size of 1 × 1 μm^2 and a *Z* scale of 40 nm.

on A_6K and V_6K self-assembled nanostructures using AFM. In the case of A_6K (Fig. 2a–2c), regardless of the kind of salt present, all three peptide-salt complexes (carbonates, sulfates, and phosphates) formed nanotube structures that show slightly larger heights, 4.5 nm for carbonate, 2.9 nm for sulfate, and 3.2 nm for phosphate ion, respectively (Fig. S4a–c, ESI†). Compared with the self-assemblies formed by the carbonate or sulfate anion systems, the phosphate anions enhance the formation of nanofibers with higher density of distribution, indicating a stronger interaction between A_6K and phosphate ions. Similarly, the nanostructure of the V_6K self-assemblies was verified with respect to the three different anions (Fig. 2d–2f). In the presence of carbonate and sulfate ions, the primary aggregates can fuse and grow into nanofibers with heights of 5.3 nm and 3.9 nm, respectively, in which random bending along the long fibrillar axis is the dominant conformation. However, for phosphate ions, numerous long nanofibers approximately 7.5 nm tall appeared to cross over (Fig. S4d–f, ESI†), indicating that the peptide/phosphate ion system favors axial growth and a different mode of ion interaction.

CD measurements were performed to help assess the effects of different counterions on peptide conformation within the assembled nanostructures (Fig. 3). The secondary structure of A_6K in the presence of different counterions displays a negative minimum at approximately 197 nm, revealing the predominance of random coil conformation in all cases (Fig. 3a). The CD spectrum of V_6K in the presence of different counterions (Fig. 3b) is similar to that of V_6K without any added anions despite the morphological variations. Considering that all peptides possess similar secondary structures but self-assemble into various nanostructures in water, we listed the negative peak shifts in the different cases (Table 1, ESI†) using the CD spectrum of A_6K and V_6K (Fig. 1e

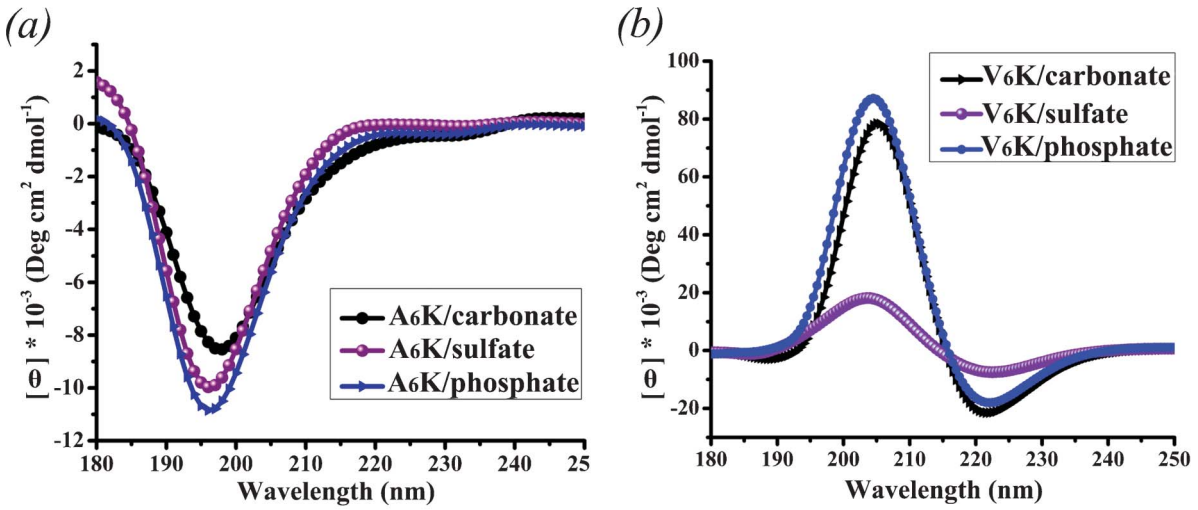

Fig. 3 CD spectra measured from (a) A_6K and (b) V_6K in the presence of different sodium salts.

and 1f) as reference points. The introduction of carbonate and sulfate anions caused moderate peak shifts, whereas phosphate ions caused the largest peak shifts (−10 and 2 nm, respectively), suggesting strong interactions between the peptide and phosphate anions. These observations, together with the AFM characterization, demonstrate that the phosphate ions induce a stronger influence compared with carbonate or sulfate anions, and there are different mechanisms of ion effects in tuning peptide aggregation. The interaction between peptides and multivalent anions is a complicated process, and such counterions can affect peptide self-assembly through a complicated combination of ion binding and electrostatic screening. This combination can further affect hydrophobic interaction and dispersion forces. Carbonate and sulfate ions tend to coordinate with weak positively charged residues on peptides because they have low surface charge densities and are weakly hydrated in solution.[40,41] Xu *et al.*[42] also showed that the phosphate ions with high surface charge densities are strongly hydrated in solution, and thus move away from the weak positively charged residues on peptides. These observations suggest that the structures and sizes of the peptide self-assemblies depend significantly on the type of counterions used, which agrees with previous studies that the peptide self-assembly process can be modulated by various environmental triggers.[43–47]

3.3 Biosilica formation by A_6K and V_6K

The formation of a peptide/anion complex is an important factor in the production of ordered silica structures. Thus, it is useful to compare the morphology of the silica structures in the absence and presence of counterions (Fig. 4). In the control experiments, the absence of any anions only produced fibrillar structures with non-uniform lengths (Fig. 4a and 4b). We investigated the effect of three types of counterions (carbonate, sulfate, and phosphate ions) on biosilica formation. Upon the addition of silicic acid and when using carbonate as a counterion there is a profound influence on the resulting biosilica morphologies. The corresponding SEM images (Fig. 4c and 4d) show that flower-like biosilica structures consisting of lamellar layers were obtained from A_6K, whereas fibrillar structures were obtained from V_6K. By

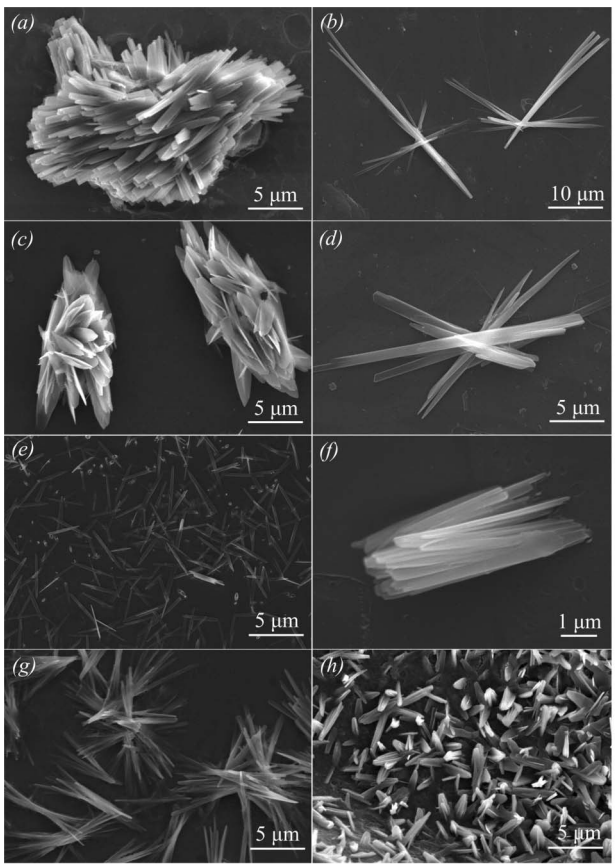

Fig. 4 Effects of the peptide molecular composition and counterions on the biosilica structure. Scanning electron microscopy (SEM) images of biosilica directed by (a) A_6K, (b) V_6K, (c) A_6K/carbonate, (d) V_6K/carbonate, (e) A_6K/sulfate, (f) V_6K/sulfate, (g) A_6K/phosphate, and (f) V_6K/phosphate.

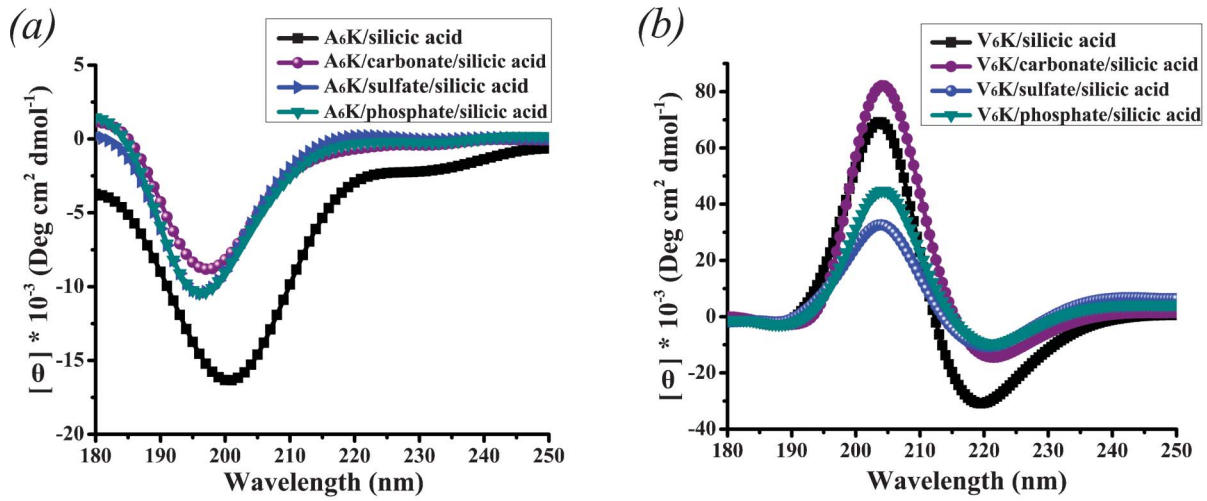

Fig. 5 CD spectra of the silicification system of (a) A_6K and (b) V_6K in the absence and presence of different sodium salts.

contrast, using the same reaction conditions and procedures, we replaced the carbonate ions with sulfate and phosphate ions, and found that fibrillar structures were obtained from A_6K, and stacks were obtained from V_6K, respectively (Fig. 4e–4h).

Observing the variation and novel silica morphologies with respect to types of anions was more interesting compared with the self-assemblies formed by the peptide/anions system (Fig. 2). These observations suggest that the nucleation of silicic acid is not only related to the type of counterion, but also relies on electrostatic interactions between the negatively charged silica intermediates and the positively charged peptide surface.[26,48] This relationship indicates that introducing anions is necessary but not sufficient to fabricate biosilica with novel morphologies. Changes in size and hydrophobicity allow us to assess the influence of size and hydrophobicity of the peptides tails on self-assembly and biomineralization. As V_6K has a higher aggregating ability than A_6K, the fibrils self-assembled by V_6K show a stronger aggregation tendency,[15,18] which results in the formation of biosilica with lamellar bilayer structures in sulfate and phosphate anions (Fig. 4f and 4h, respectively). The hydrogen-bonded network of the self-assembled template and the electrostatic interactions are supposedly responsible for interfacial molecular recognition at the organic/inorganic interface during crystallization.[33,49–51] Therefore, biosilica materials with controlled morphologies can be obtained by selecting different types of anions or varying the peptide composition. These results agree with a previous report, in which an amphiphilic poly(L-lysine)-*block*-poly(L-leucine) diblock copolypeptide and its supramolecular assembly were used as organic templates to direct silica formation, thereby suggesting that multiple morphologies can be controlled by changing the type of counterion.[52]

The CD spectra of the biosilica particles were recorded to characterize the conformation of A_6K and V_6K in the composites (Fig. 5). Without any counterion added, the spectra for the A_6K/silicic acid systems display a strong negative minimum around 200 nm, which suggests a primary random coil conformation. In the case of the V_6K/silicic acid system, the CD spectrum has a positive maximum at about 205 nm and a negative minimum at 220 nm, which are characteristic of β-sheet formation. Therefore, comparing with the CD spectrum of both peptide solutions in pure water (Fig. 1e and 1f), the introduction of silicic acid caused negligible changes except for a strengthening in the biomimetic systems. Similarly, upon the addition of various counterions such as carbonate, sulfate, and phosphate ions, no obvious changes in the shape of the CD spectra were observed in spite of morphological variations (Fig. 4c–4h), indicating that the counterions were not sufficient to induce a secondary structural transition. These observations imply that A_6K and V_6K self-assemblies were successfully employed during the fabrication of silica *via* templating.

To further understand the function of an externally applied force in the facilitation of biosilica precursor deposition,

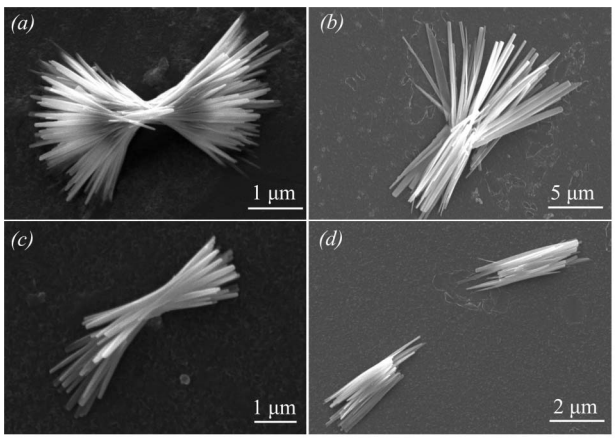

Fig. 6 Effects of peptide molecular composition and external conditions on biosilica structures. SEM images of biosilica directed by (a) A_6K under electrostatic field, (b) A_6K under flow field, (c) V_6K under electrostatic field, and (d) V_6K under flow field. The additive anion is phosphate.

external electrostatic and flow fields were introduced as powerful energy sources to direct the peptide self-assembly and to promote ordered material synthesis using phosphate as the additive anion for all samples (Fig. 6). Lysine with a different hydrophobic tail could form a similar biosilica with fibrillar structures, except for the diameter and length. For example, in the presence of electrostatic fields, the A_6K/phosphate system produces biosilica fibers about 500 to 700 nm wide and 5 to 10 μm long (Fig. 6a), whereas the products formed by the V_6K/phosphate system are approximately 200 nm in width and over 10 μm long (Fig. 6c). Comparing the same reactants in the absence of any externally applied force fields, we were able to direct biosilica formation to produce a more uniform morphology through careful manipulation of the physical reaction environment and through mechanical force. The surfactant-like self-assembly rules are generally applicable in the presence of external force fields, and possibly in selectively precipitating biosilica with controlled morphologies that are not realized by other methods.[30,31]

The FT-IR spectra of the A_6K and V_6K molecules and the biosilica materials are shown in Fig. 7. For the A_6K-silica composite, the hybrid silica displays three characteristic peaks: –Si–O–Si– asymmetric stretching at 1052 cm^{-1}, symmetric stretching at 802 cm^{-1}, and Si–OH stretching at 967 cm^{-1}. Furthermore, two other characteristic bands were observed at 1628 and 1532 cm^{-1}, which are attributed to amide I (νC=O) and amide II (δN–H) bands from the peptide, respectively. A similar analysis was performed for the V_6K-silica system, which shows the characteristic peaks as follows: –Si–O–Si– asymmetric stretching at 1085 cm^{-1}, symmetric stretching at 793 cm^{-1}, and Si–OH stretching at 959 cm^{-1}. Similarly, two other characteristic bands at 1654 and 1549 cm^{-1} were also observed, which are attributed to amide I (νC=O) and amide II (δN–H) bands from the peptide, respectively. These results suggest that the β-sheet structure is present in the majority of the A_6K/silicic acid and the V_6K/silicic acid systems, which agrees well with the CD results. TGA was also used to determine the amount of soft template in the

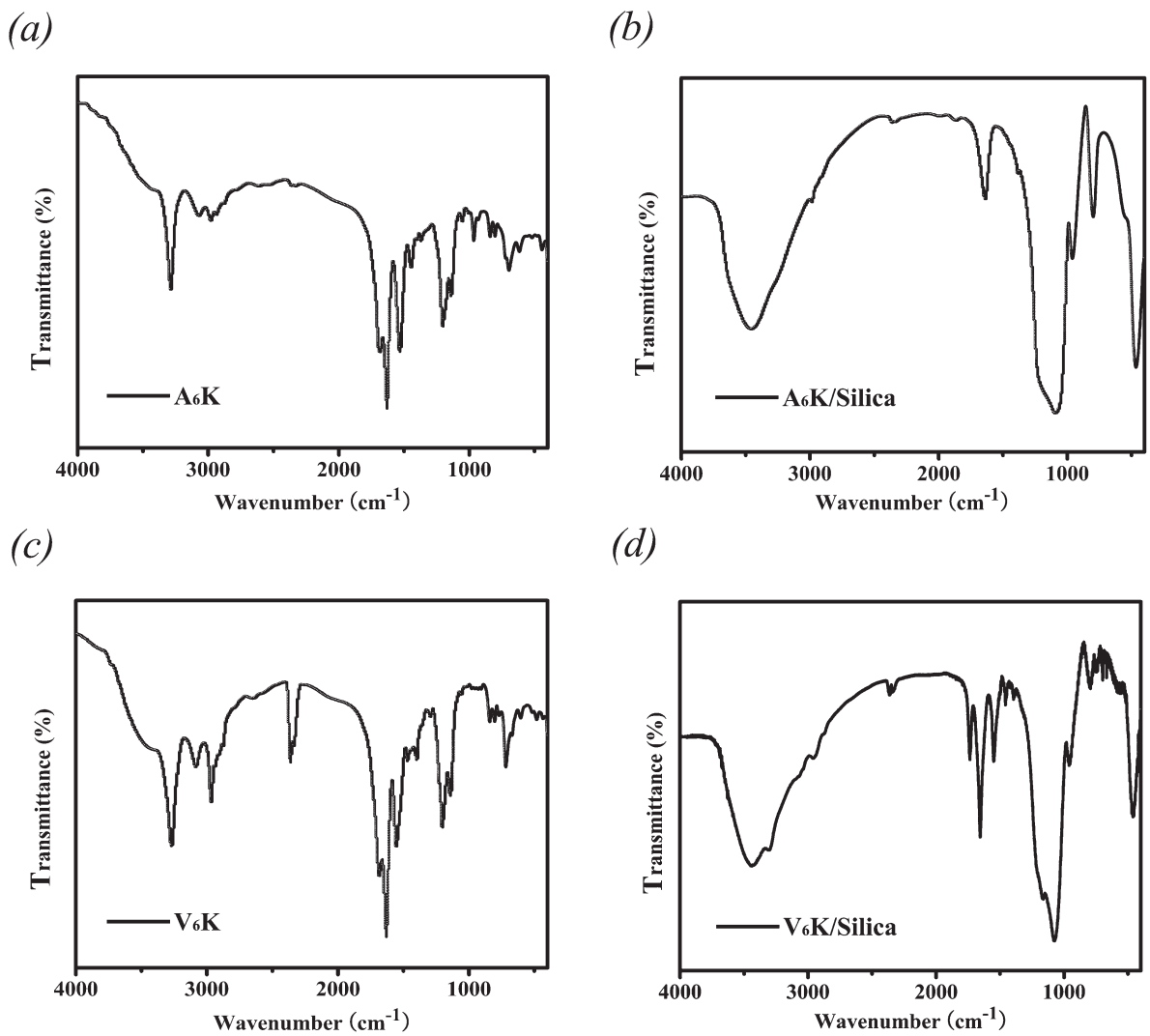

Fig. 7 Fourier transformed infrared (FT-IR) spectra of (a) A_6K, (b) A_6K/silica, (c) V_6K, and (d) V_6K/silica.

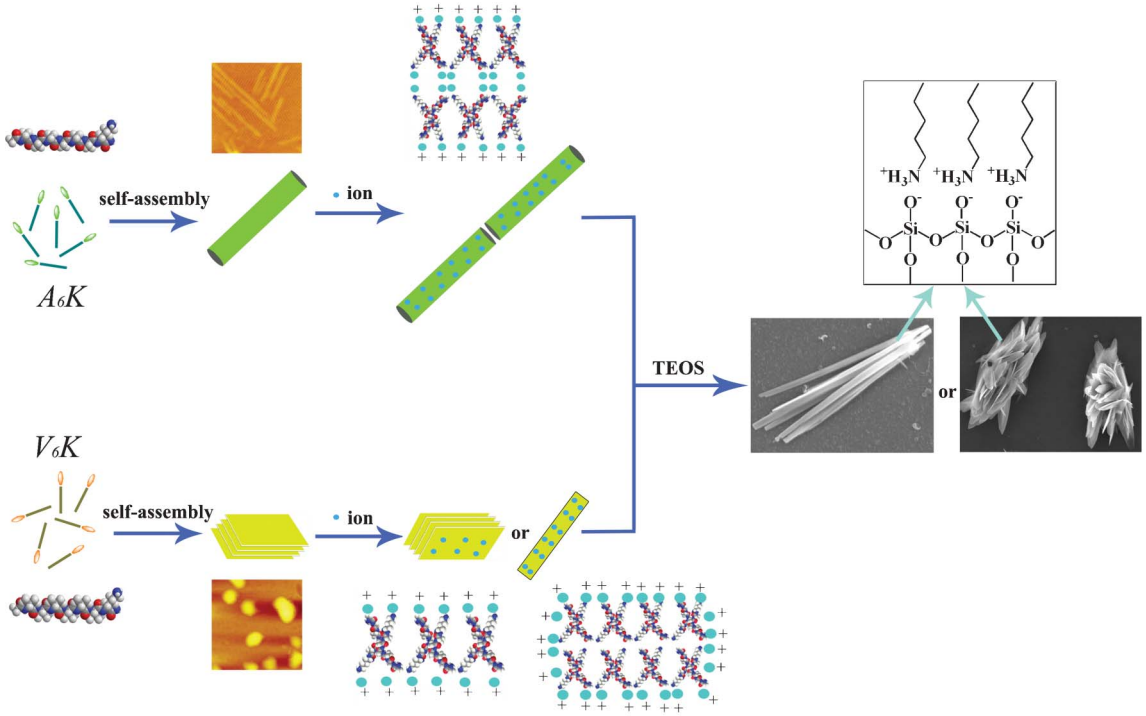

Fig. 8 A schematic illustration of templating biosilica deposition directed by the self-assembled short peptides A_6K and V_6K.

as-synthesized particles (Fig. S5, ESI†). The dominant weight losses occurred at around 250 to 500 °C and 300 to 420 °C, respectively. The organic contents of A_6K/silicic acid systems (70%) are higher than those of V_6K/silicic acid systems (62%) due to the different peptide concentration used in the experiments. Therefore, these observations confirm the entrapment of the A_6K and V_6K peptide into silica formed *via* templating.

Our proposed model for biosilica formation using A_6K and V_6K self-assemblies as templates is shown in Fig. 8. In aqueous solutions, A_6K self-assembled into nanotubes 2.7 nm tall and approximately 1 to 2 μm long. However, due to an increase in molecular hydrophobicity, V_6K molecules self-assembled into lamellar stacks that were 4 nm tall and under 100 nm long. In the present system, the anion effects on peptide morphologies can be divided into two categories. For A_6K, the addition of counterions in all cases led to nanotube aggregation and an increase in nanotube length from 2 μm to over 5 μm. The final nanotubes resembled strings of sausages. In contrast, in the case of V_6K, the introduction of anions significantly influenced the peptide self-assemblies. The carbonate and sulfate ions favor the formation of short nanofibers, whereas the phosphate ions enhance the peptide growth into larger clubbed structures. Under the effects of various ions, the lamellar stacks self-curl to form short nanofibers or nanorods due to the different electrostatic repulsions between the surface lysine residues. Finally, chemical and physical factors that may affect the morphologies of biosilica structures were systematically studied. Upon the addition of silicic acid to the peptide/anion mixtures, the A_6K and V_6K self-assemblies in aqueous solution can quickly adjust their corresponding aggregation patterns after interacting with the counterions and silicic acid, and then grow accordingly into ordered templates to tailor biosilica formation with different morphologies. The anions are used as "spacers" in between self-assemblies and silica precursors, serving as structure-directing agents. Comparing with the self-assembled structures formed by the peptide/anions system, novel silica morphologies such as flower-like, fibrillar, and lamellar structures, are obtained after the introduction of silicic acid. The formation of a peptide/anion complex was necessary but not enough to produce well-defined biosilica materials with novel morphologies under mild conditions. In addition, as V_6K has a higher aggregation ability than A_6K, the fibrils self-assembled with V_6K show stronger aggregation tendency, leading to the formation of biosilica with lamellar bilayer structures. Interestingly, when external electrical or flow fields were applied in the biomimetic experiment, only fibrillar biosilica structures were found. Thus, biosilica materials with controlled morphologies can be obtained through careful adjustment of chemical and physical factors such as the peptide composition, the nature of peptide/anion complex, and the application of external electrostatic/flow fields.

4. Conclusions

We have described a versatile and easily controlled method using two amphiphilic peptides, A_6K and V_6K self-assemblies, as organic templates to direct the formation of structural silica with controlled morphologies. In aqueous solution, A_6K self-assembled into nanofibers, whereas V_6K self-assembled into

lamellar stacks nanostructures. The effects of adding counterions to these two amphiphilic peptide solutions were studied. Our findings show that the phosphate ions have a stronger influence in tuning the nanostructures and lengths compared with carbonate and sulfate ions. Furthermore, we systematically investigated several chemical/physical factors such as the peptide composition, the nature of peptide/anion complexes, and the application of external fields on the resulting biosilica morphologies. By adjusting the silication conditions, biosilica with multiple morphologies can be easily tuned under different conditions, which introduces a new avenue for forming hierarchical, ordered inorganic materials using assembled templates.

Acknowledgements

This work was supported by the National Natural Science Foundation of China (20871080, 50973058), the Team Project of the Natural Science Foundation of Guangdong Province (9351503102000001) and the Innovation Team Construction Project of Shantou University (ITC11002).

References

1 S. G. Zhang, *Nat. Biotechnol.*, 2003, **21**, 1171.
2 E. Kokkoli, A. Mardilovich, A. Wedekind, E. L. Rexeisen, A. Garga and J. A. Craig, *Soft Matter*, 2006, **2**, 1015.
3 L. Adler-Abramovich, D. Aronov, P. Beker, M. Yevnin, S. Stempler, L. Buzhansky, G. Rosenman and E. Gazit, *Nat. Nanotechnol.*, 2009, **4**, 849.
4 H. G. Cui, M. J. Webber and S. I. Stupp, *Biopolymers.*, 2010, **94**, 1.
5 D. N. Woolfson and Z. N. Mahmoud, *Chem. Soc. Rev.*, 2010, **39**, 3464.
6 I. W. Hamley, *Soft Matter*, 2011, **7**, 4122.
7 M. Y. Xie, H. Li, M. Ye, Y. Zhang and J. Hu, *J. Phys. Chem. B*, 2012, **116**, 2927.
8 S. Santoso, W. Hwang, H. Hartman and S. G. Zhang, *Nano Lett.*, 2002, **2**, 687.
9 G. V. Maltzahn, S. Vauthey, S. Santoso and S. G. Zhang, *Langmuir*, 2003, **19**, 4332.
10 H. Xu, J. Wang, S. Y. Han, J. Q. Wang, D. Y. Yu, H. Y. Zhang, D. H. Xia, X. B. Zhao, T. A. Waigh and J. R. Lu, *Langmuir*, 2009, **25**, 4115.
11 J. Wang, S. Y. Han, G. Meng, H. Xu, D. H. Xia, X. B. Zhao, R. Schweins and J. R. Lu, *Soft Matter*, 2009, **5**, 3870.
12 X. B. Zhao, F. Pan, S. Perumal, H. Xu, J. R. Lu and J. R. P. Webster, *Soft Matter*, 2009, **5**, 1630.
13 S. Bucak, C. Cenker, I. Nasir, U. Olsson and M. Zackrisson, *Langmuir*, 2009, **25**, 4262.
14 X. B. Zhao, F. Pan, H. Xu, M. Yaseen, H. H. Shan, C. A. E. Hauser, S. G. Zhang and J. R. Lu, *Chem. Soc. Rev.*, 2010, **39**, 3480.
15 F. Pan, X. B. Zhao, S. Perumal, T. A. Waigh and J. R. Lu, *Langmuir*, 2010, **26**, 5690.
16 S. Y. Han, S. S. Cao, Y. M. Wang, J. Q. Wang, D. H. Xia, H. Xu, X. B. Zhao and J. R. Lu, *Chem.–Eur. J.*, 2011, **17**, 13095.
17 Q. B. Meng, Y. Y. Kou, X. Ma, Y. J. Liang, L. Guo, C. H. Ni and K. L. Liu, *Langmuir*, 2012, **28**, 5017.
18 S. Y. Han, W. W. Xu, M. W. Cao, J. Q. Wang, D. H. Xia, H. Xu, X. B. Zhao and J. R. Lu, *Soft Matter*, 2012, **8**, 645.
19 S. C. Holmström, P. J. S. King, M. G. Ryadnov, M. F. Butler, S. Mann and D. N. Woolfson, *Langmuir*, 2008, **24**, 11778.
20 A. Altunbas, N. Sharma, M. S. Lamm, C. Yan, R. P. Nagarkar, J. P. Schneider and D. J. Pochan, *ACS Nano*, 2010, **4**, 181.
21 M. Reches and E. Gazit, *Curr. Nanosci.*, 2006, **2**, 105.
22 S. V. Patwardhan, *Chem. Commun.*, 2011, **47**, 7567.
23 X. F. Zhou, L. F. Zheng, R. Li, B. Li, S. Pillai, P. Xu and Y. Zhang, *J. Mater. Chem.*, 2012, **22**, 8862.
24 V. M. Yuwono and J. D. Hartgerink, *Langmuir*, 2007, **23**, 5033.
25 H. Xu, Y. Wang, X. Ge, S. Han, S. Wang, P. Zhou, H. Shan, X. Zhao and J. R. Lu, *Chem. Mater.*, 2010, **22**, 5165.
26 S. J. Wang, X. Ge, J. Y. Xue, H. M. Fan, L. J. Mu, Y. P. Li, H. Xu and J. R. Lu, *Chem. Mater.*, 2011, **23**, 2466.
27 S. J. Wang, J. Y. Xue, X. Ge, H. M. Fan, H. Xu and J. R. Lu, *Chem. Commun.*, 2012, **48**, 9415.
28 R. Wieneke, A. Bernecker, R. Riedel, M. Sumper, C. Steinem and A. Geyer, *Org. Biomol. Chem.*, 2011, **9**, 5482.
29 J. Yi, H. S. Jang, J. S. Lee and W. I. Park, *Nano Lett.*, 2012, **12**, 3743.
30 R. R. Naik, P. W. Whitlock, F. Rodriguez, L. L. Brott, D. D. Glawe, S. J. Clarson and M. O. Stone, *Chem. Commun.*, 2003, 238.
31 F. Rodriguez, D. D. Glawe, R. R. Naik, K. P. Hallinan and M. O. Stone, *Biomacromolecules*, 2004, **5**, 261.
32 D. D. Glawe, F. Rodriguez, M. O. Stone and R. R. Naik, *Langmuir*, 2005, **21**, 717.
33 L. Xia and Z. B. Li, *Langmuir*, 2011, **27**, 1116.
34 F. F. Wang, F. Jiang, Y. Li, Q. R. Wang and X. Zhang, *RSC Adv.*, 2012, **2**, 5738.
35 S. E. Paramonov, H. W. Jun and J. D. Hartgerink, *J. Am. Chem. Soc.*, 2006, **128**, 7291.
36 F. Versluis, H. R. Marsden and A. Kros, *Chem. Soc. Rev.*, 2010, **39**, 3434.
37 A. L. Boyle and D. N. Woolfson, *Chem. Soc. Rev.*, 2011, **40**, 4295.
38 F. Qiu, Y. Z. Chen, C. K. Tang, Q. H. Zhou, C. Wang, Y. K. Shi and X. J. Zhao, *Macromol. Biosci.*, 2008, **8**, 1053.
39 F. Qiu, Y. Z. Chen and X. J. Zhao, *J. Colloid Interface Sci.*, 2009, **336**, 477.
40 K. D. Collins, *Methods*, 2004, **34**, 300.
41 K. D. Collins, G. W. Neilson and J. E. Enderby, *Biophys. Chem.*, 2007, **128**, 95.
42 M. W. Cao, Y. M. Wang, X. Ge, C. H. Cao, J. Wang, H. Xu, D. H. Xia, X. B. Zhao and J. R. Lu, *J. Phys. Chem. B*, 2011, **115**, 11862.
43 S. J. Siegel, J. Bieschke, E. T. Powers and J. W. Kelly, *Biochemistry*, 2007, **46**, 1503.
44 R. Verel, I. T. Tomka, C. Bertozzi, R. Cadalbert, R. A. Kammerer, M. O. Steinmetz and B. H. Meier, *Angew. Chem., Int. Ed.*, 2008, **47**, 5842.
45 J. N. Shera and X. S. Sun, *Biomacromolecules*, 2009, **10**, 2446.
46 V. Castelletto, I. W. Hamley, C. Cenker and U. J. Olsson, *J. Phys. Chem. B*, 2010, **114**, 8002.

47 S. Lei, J. Zhang, J. R. Wang and J. B. Huang, *Langmuir*, 2010, **26**, 4288.
48 A. F. Wallace, J. J. DeYoreo and P. M. Dove, *J. Am. Chem. Soc.*, 2009, **131**, 5244.
49 S. Mann, *Nature*, 1988, **332**, 119.
50 M. Sarikaya, C. Tamerler, A. K. Y. Jen, K. Schulten and F. Baneyx, *Nat. Mater.*, 2003, **2**, 577.
51 F. K. Wang, S. L. Nimmo, B. R. Cao and C. B. Mao, *Chem. Sci.*, 2012, **3**, 2639.
52 L. Xia, Y. Liu and Z. B. Li, *Macromol. Biosci.*, 2010, **10**, 1566.